atoms

MDPI

Article

Partial Photoionization Cross Sections of Chromium from the Ground and Excited States

Oleg Zatsarinny [1,*,†] and Swaraj Tayal [2,†]

[1] Department of Physics and Astronomy, Drake University, Des Moines, IA 50311, USA
[2] Department of Physics, Clark Atlanta University, Atlanta, GA 30314, USA; stayal@cau.edu
* Correspondence: oleg.zatsarinny@drake.edu
† These authors contributed equally to this work.

Received: 20 July 2020; Accepted: 24 August 2020; Published: 27 August 2020

Abstract: Partial and total photoionization cross sections of iron-peak elements are important for the determination of abundances in late-type stars and nebular objects. We have investigated photoionization of neutral chromium from the ground and excited states in the low energy region from the first ionization threshold at 6.77 eV to 30 eV. Accurate descriptions of the initial bound states of Cr I and the final residual Cr II ionic states have been obtained in the multiconfiguration Hartree-Fock method together with adjustable configuration expansions and term-dependent non-orthogonal orbitals. The *B*-spline *R*-matrix method has been used for the calculation of photoionization cross sections. The 194 *LS* final ionic states of Cr II $3d^4 4s$, $3d^3 4s^2$, $3d^5$, $3d^4 4p$, and $3d^3 4s 4p$ principal configurations have been included in the close-coupling expansion. The inclusion of all terms of these configurations has significant impact on the near-threshold resonance structures as well as on the nonresonant background cross sections. Total photoionization cross sections from the ground $3d^5 4s\ a^7S$ and excited $3d^5 4s\ a^5S$, $3d^4 4s^2\ a^5D$, $3d^5 4p\ z^5P$, and $3d^4 4s 4p\ y^5P$ states of Cr I have been compared with other available *R*-matrix calculation to estimate the likely uncertainties in photoionization cross sections. We analyzed the partial photoionization cross sections for leaving the residual ion in various states to identify the important scattering channels, and noted that $3d$ electron ionization channel becomes dominant at higher energies.

Keywords: atomic spectroscopy; photoionization; transition probabilities

PACS: 32.80.Fb; 31.15.Em

1. Introduction

Radiative transition probabilities and low-energy photoionization processes have important applications in several fields of science such as astrophysics, plasma physics, atmospheric science, and lighting industry. Chromium (Cr I, Z = 24) belongs to the iron group and is characterized by the $3d^5 4s$ ground configuration. Cosmic abundances of the transition metals Sc-Ni ($21 \leq Z \leq 28$) tend to form a "peak" around iron. Variation of abundances within the group provides information on nuclear physics and the physical environments in which the elements were processed. Accurate abundances are the key components necessary to understand stellar chemical evolution. The derivation of reliable abundances requires precise atomic data. In particular, accurate photoionization cross sections and transition probabilities for iron group elements are needed for the modeling of measured spectra from the late-type stars [1–3]. The partial photoionization cross sections from the ground and low-lying excited states are usually important for nonlocal thermodynamic equilibrium modeling. Due to the scarcity of experimental studies on electron and photon collisions with the transition elements, the atomic data needs for the analysis and modeling of astrophysical plasmas have been mostly fulfilled

by theoretical and computational investigations. In addition to practical applications, photoionization studies can provide a better understanding of dynamical effects due to electron correlation and interchannel coupling effects in open 3*d*-shell atomic systems.

Photoionization of 3*d* transition metal atoms from Sc to Cu attracted special attention and has been the subject of a set of experimental studies, using different approaches, such as photoabsorption, photoelectron Auger electron, photo-ion-yield and fluorescence spectroscopy. Several excellent review papers are available, in particular, Martins et al. [4] summarized photoionization studies of 3*d* atoms. All studies concentrated on the core photoionization of 3*s* and 3*p* electrons, with photon energy range from 30 to 70 eV. Interest to this energy region was mostly caused by the prominent $3p - 3d$ resonances. In particular, the 3*p* photoabsorption spectrum of Cr I is composed of a broad resonance at 43.9 eV and a number of strong and sharp lines lying below and above the $3p - 3d$ broad resonance. Considerable experimental efforts had been made to investigate and understand the 3*p* absorption spectra of Cr I [5–9]. Theoretical studies have also been performed to understand and reproduce the experimental 3*p* absorption feature of Cr I [10,11].

The low-energy photoionization of Cr I for photon energies between the first ionization threshold at 6.77 eV and 30 eV received much less attention both from theory and experiment. We are not aware of any experimental study in the low-energy range below 30 eV. Early theoretical calculations of photoionization were performed using the Hartree-Dirac-Slater central-field method [12] and Hartree-Dirac-Slater central-field method together with a simple fitting procedure [13]. The only extensive calculation of the Cr I photoionization in the low-energy region has been reported by Nahar [14]. Using the unified method based on the close-coupling approximation and *R*-matrix method [15], the photoionization and inverse electron-ion recombination processes were studied in detail for neutral chromium, (Cr I + $h\nu \leftrightarrow$ Cr II + e), for the ground and excited states. Results are presented for the septet and quintet states with $n \leq 10$ and $l \leq 9$. Structures in the total and partial photoionization cross sections for ionization into various excited core states and ground state were demonstrated. Calculations were carried out in *LS* coupling by including 40 ionic states in the close-coupling wave function expansion. The results were estimated to provide sufficiently accurate values of photoionization and recombination cross sections for modeling calculations. However, the author also indicated the possible corrections due to more extended treatment of electron correlation and close-coupling effects. The convergence of the available photoionization cross sections for Cr I is still an open question.

The ground and excited configurations of chromium with an open 3*d* shell give rise to many possible terms resulting in a very complex spectrum, and photoionization and transition probabilities calculations become extremely cumbersome. The existing calculations include only a small part of the Cr I spectrum, raising questions regarding the convergence of the results. The purpose of the present work is to perform more elaborate and extensive calculations for photoionization of Cr I than the available calculations and, thereby, check the convergence of the predicted cross sections. Our detailed investigations include the dependence of cross sections on the scattering model and the accuracy of the initial Cr I bound states and final residual ionic Cr II target wave functions.

In the present work, we employed the *B*-spline *R*-matrix (BSR) method [16]. The reliable photoionization calculation requires an accurate account of a variety of correlation and relaxation effects in the description of Cr I bound states, final continuum states, and Cr II residual ionic target states. Therefore, first of all we have attempted to improve the target wave functions by using flexible nonorthogonal sets of orbitals to describe term-dependence of valence orbitals as well as correlation and relaxation effects. The multiconfiguration Hartree-Fock (MCHF) method with adjustable configuration expansions to include all important correlation corrections was used to generate accurate target wave functions. We used *B*-spline basis for the description of continuum functions, and no orthogonality constraint between continuum functions and the valence spectroscopic and correlation orbitals was imposed. This allowed us to avoid potential inconsistencies between the continuum and bound parts of the close-coupling expansions. This is important for generating the near-threshold resonances with

correct positions and magnitudes. The flexibility and accuracy of the BSR was demonstrated in our recent calculations for photoionization of Fe I [17] and electron collisions with Fe II [18] and Fe I [19].

The present calculations include the photoionization of valence $3d$, $4s$, and $4p$ electrons from the atomic chromium initial bound terms of the $3d^5 4s$, $3d^4 4s^2$, $3d^5 4p$, and $3d^4 4s 4p$ configurations giving rise to the final singly-ionized chromium terms of the $3d^4 4s$, $3d^3 4s^2$, $3d^5$, $3d^4 4p$, and $3d^3 4s 4p$ configurations. We have included all 194 *LS* states of these ionic configurations in the close-coupling expansion and, therefore, we attempted to cover *all* major photoionization channels. The resulting close-coupling expansions include sufficient number of states to very likely provide converged photoionization cross sections. The calculations are performed across all the Rydberg series of resonances converging to various ionic thresholds. Inclusion of electron correlation effects in a consistent manner both in the initial bound and final continuum states ensures accurate description of resonance structures. We have found that the inclusion of all states of the $3d^4 4p$ and $3d^3 4s 4p$ configurations has considerable influence on the low-energy resonance structures and on the energy dependence of the photoionization cross sections, especially for photoionization of the excited states. The comparison of our calculations with other available results is used to provide an estimate of likely uncertainties in the existing photionization cross sections data sets.

2. Computational Methods

2.1. Initial Bound and Final Ionic States Wave Functions

The near degeneracy of the states of $3d^x$, $3d^{x-1}4s$, $3d^{x-2}4s^2$ and other configurations for the neutral chromium and its singly-charged ion give rise to a very complicated atomic structure with a large number of terms. The complexity of the atomic structure is further increased by the overlap of terms belonging to different configurations. The calculation and analysis of such a complex spectrum are challenging tasks. The description of electron correlation effects requires to consider at least single and double promotions of the valence electrons to excited orbitals in the configuration expansions, leading to very large expansions that are extremely difficult to deal with using standard atomic structure methods. Our atomic structure calculations have been performed using the MCHF code of Froese Fischer [20] in combination with configuration-interaction codes [21,22] with nonorthogonal orbitals. These calculations are similar to the structure calculations in our recent works on the photoionization of Fe I [17] and on electron collisions with Fe II [18] and Cr II [23] where the computational details can be found. Here we provide only the specific aspects of the present calculations.

There are two important distinguishable features of our calculations of atomic wave functions. Firstly, we use flexible term-dependent non-orthogonal sets of radial functions for the multiconfiguration description of different initial bound and residual final ionic states accurately. In principle, a similar accuracy can be achieved with an orthogonal set of one-electron orbitals, but it will require very large configuration expansions using additional correlated pseudo-orbitals. The term dependence of the valence orbitals, both in Cr I and Cr II was found to be noticeable with a maximum change of the mean radius for the $3d$ electron up to 15%, resulting in corrections of about 2.7 eV in the term energies. Thus the term dependence is very important for accurate calculations of various term energies both of neutral and singly-charged chromium. The second important feature of our approach is the inclusion of all major electron correlation effects by properly choosing dominant configurations from thousands of individual atomic configurations generated by all possible one- and two-electron promotions of the valence $3d$, $4s$, and $4p$ orbitals of the principal configurations. This was accomplished by analyzing full configuration expansion for a given term and by choosing configurations with significant expansion coefficients. As result, the final configuration expansions include all important electron correlation and, at the same time, they are of manageable size for the following photoionization calculations. The various atomic states were found to show very different convergence rates. We noted faster convergence for septet and quintet states, but a slower convergence

pattern for the singlet and triplet states, especially for the $4s4p$ configuration. For this reason, we used different cut-off parameters in the range from 0.008 to 0.020 for the various atomic-states configuration expansions. Such procedure also allows us to fine-tune the theoretical LS energies to the weighted average of the experimental fine-structure levels energies from the NIST compilation [24]. The final configuration expansions for the target states in the present work have size between 400 and 1200 and could be handled using the available high performance computational facilities.

Table 1 compares the calculated LS excitation energies for the 20 bound states of neutral chromium considered in the present photoionization calculations with the experimental excitation energies from the NIST compilation [24]. It is clear from the Table that the approach described above yields very accurate theoretical energies. The agreement with the observed LS energies is better than 0.1 eV for all 20 bound states. In our final photoionization calculations we have used experimental binding energies for the chromium states to further improve the positions of related autoionizing states.

Table 1. Excitation energies (in eV) of the Cr I target levels included in the present photoionization calculations.

Index	Configuration	Term	Present	NIST [24]	Diff.
1	$3d^5(^6S)4s$	$a\,^7S$	0.00000	0.00000	0.000
2	$3d^5(^6S)4s$	$a\,^5S$	0.96834	0.94143	0.027
3	$3d^44s^2$	$a\,^5D$	1.07316	1.00306	0.070
4	$3d^5(^4G)4s$	$a\,^5G$	2.58104	2.54433	0.037
5	$3d^5(^4P)4s$	$a\,^5P$	2.73922	2.70861	0.031
6	$3d^44s^2$	$a\,^3P$	2.99331	2.95034	0.043
7	$3d^5(^6S)4p$	$z\,^7P^o$	2.90405	2.90311	0.001
8	$3d^44s^2$	$a\,^3H$	3.04260	2.98548	0.057
9	$3d^5(^4D)4s$	$b\,^5D$	3.05242	3.01185	0.041
10	$3d^5(^4G)4s$	$a\,^3G$	3.15106	3.09197	0.062
11	$3d^44s^2$	$a\,^3F$	3.19426	3.11167	0.083
12	$3d^4(^5D)4s4p$	$z\,^7F^o$	3.16239	3.15322	0.009
13	$3d^5(^6S)4p$	$z\,^5P^o$	3.32659	3.32194	0.005
14	$3d^5(^4P)4s$	$b\,^3P$	3.40577	3.37245	0.033
15	$3d^4(^5D)4s4p$	$z\,^7D^o$	3.44164	3.42281	0.019
16	$3d^44s^2$	$b\,^3G$	3.51032	3.43711	0.073
17	$3d^4(^5D)4s4p$	$y\,^7P^o$	3.46362	3.45268	0.011
18	$3d^5(^4D)4s$	$a\,^3D$	3.65845	3.55345	0.105
19	$3d^4(^5D)4s4p$	$y\,^5P^o$	3.69098	3.67785	0.013
20	$3d^4(^5D)4s4p$	$z\,^5F^o$	3.87109	3.85220	0.018

Comparison of radiative data, such as radiative rates and lifetimes, provides another strong opportunity to estimate the accuracy of the target expansions. The comprehensive review of available oscillator strengths data sets for the iron group elements Sc to Ni was provided by Scott et al. [25] in their study of the elemental composition of the Sun. For comparison of oscillator strengths in Cr I we choose the most recent study of Sobeck et al. [26], who measured branching fractions and normalised them with the extensive and accurate time-resolved laser-induced fluorescence lifetimes of Cooper et al. [27]. We have calculated radiative lifetimes and transition probabilities between fine-structure levels by including the spin-orbit mixing in our LS wave functions and compared present results with experimental values in the Table 2. The comparison shows a good agreement with experimental values. The average deviation between the present and experimental lifetimes is about 10%, whereas the deviation for the oscillator strengths is approximately 20%. As typical for the radiative rates calculations, better agreement is obtained for the stronger transitions, where both sets of results agree within 10%. Weak oscillator strengths (typically $\log gf < -2$) are extremely sensitive to small changes in the atomic wave functions. For several transitions we found very strong cancellation effects in the configuration expansions. For example, the $3d^54p\,^7P$ and $3d^44s4p\,^7P$ states are strongly mixed, in proportions of 60% and 40%, respectively. This leads to reduction of transition probabilities

for the $3d^5 4p\ ^7P_{2,3,4} - 3d^5 4s\ ^7S_3$ transitions up to 50%. Overall, comparison of radiative rates shows high quality of the Cr I wave functions.

Table 2. Comparison of lifetimes (ns) and transition probabilities (10^{-6} s^{-1}) for some E1 lines of Cr I.

Upper Level	Lower Level	Lifetimes BSR	Lifetimes [27]	*A*-Values BSR	*A*-Values [26]	Upper Level	Lower Level	Lifetimes BSR	Lifetimes [27]	*A*-Values BSR	*A*-Values [26]
$3d^5 4p\ ^7P_2$	$3d^5 4s\ ^7S_3$	30.3	32.2	32.9	31.0	$3d^5 4s4p\ ^5P_3$	$3d^5 4s\ ^7S_3$	67.8	69.1	0.103	0.111
$3d^5 4p\ ^7P_3$	$3d^5 4s\ ^7S_3$	29.1	31.5	34.4	31.7		$3d^5 4s\ ^5S_2$			4.26	3.38
$3d^5 4p\ ^7P_4$	$3d^5 4s\ ^7S_3$	27.5	30.3	36.2	33.0		$3d^4 4s^2\ ^5D_2$			0.33	0.43
$3d^5 4p\ ^5P_3$	$3d^5 4s\ ^7S_3$	15.0	16.2	0.201	0.184		$3d^4 4s^2\ ^5D_3$			1.86	2.52
	$3d^5 4s\ ^5S_2$			57.0	52.1		$3d^4 4s^2\ ^5D_4$			7.1	8.0
	$3d^4 4s^2\ ^5D_2$			0.29	0.34	$3d^4 4s4p\ ^5F_1$	$3d^4 4s^2\ ^5D_0$	127	101	3.78	4.66
	$3d^4 4s^2\ ^5D_3$			1.75	2.05		$3d^4 4s^2\ ^5D_1$			3.66	4.40
	$3d^4 4s^2\ ^5D_4$			6.2	7.0		$3d^4 4s^2\ ^5D_2$			0.48	0.58
$3d^5 4p\ ^5P_2$	$3d^5 4s\ ^7S_3$	14.9	16.2	0.204	0.177		$3d^5 4s\ ^5G_2$			0.38	0.27
	$3d^5 4s\ ^5S_2$			57.0	51.9	$3d^4 4s4p\ ^5F_2$	$3d^4 4s^2\ ^5D_1$	124	99.1	4.69	5.75
	$3d^4 4s^2\ ^5D_1$			0.79	0.95		$3d^4 4s^2\ ^5D_2$			2.95	3.74
	$3d^4 4s^2\ ^5D_2$			2.84	3.45		$3d^4 4s^2\ ^5D_3$			0.284	0.326
	$3d^4 4s^2\ ^5D_3$			4.81	5.23		$3d^5 4s\ ^5G_2$			0.085	0.045
$3d^5 4p\ ^5P_1$	$3d^5 4s\ ^5S_2$	14.8	16.0	58.9	52.4		$3d^5 4s\ ^5G_3$			0.32	0.23
	$3d^4 4s^2\ ^5D_0$			1.77	2.07	$3d^4 4s4p\ ^5F_3$	$3d^4 4s^2\ ^5D_2$	120	99.9	5.62	6.90
	$3d^4 4s^2\ ^5D_1$			3.93	4.53		$3d^4 4s^2\ ^5D_3$			2.29	2.70
	$3d^4 4s^2\ ^5D_2$			3.07	3.48		$3d^4 4s^2\ ^5D_4$			0.098	0.105
$3d^4 4s4p\ ^7P_2$	$3d^5 4s\ ^7S_3$	6.0	6.6	165	151		$3d^5 4s\ ^5G_3$			0.091	0.052
$3d^4 4s4p\ ^7P_3$	$3d^5 4s\ ^7S_3$	6.1	6.6	165	151		$3d^5 4s\ ^5G_4$			0.33	0.24
$3d^4 4s4p\ ^7P_4$	$3d^5 4s\ ^7S_3$	6.1	6.6	166	152	$3d^4 4s4p\ ^5F_4$	$3d^4 4s^2\ ^5D_3$	115	94.5	6.20	8.70
$3d^4 4s4p\ ^5P_1$	$3d^5 4s\ ^5S_2$	74.3	76.6	3.14	2.34		$3d^4 4s^2\ ^5D_4$			1.20	1.51
	$3d^4 4s^2\ ^5D_0$			1.83	2.31		$3d^5 4s\ ^5G_4$			0.075	0.051
	$3d^4 4s^2\ ^5D_1$			4.08	4.85		$3d^5 4s\ ^5G_5$			0.36	0.29
	$3d^4 4s^2\ ^5D_2$			3.15	3.56	$3d^4 4s4p\ ^5F_5$	$3d^4 4s^2\ ^5D_4$	109	91.3	8.40	10.6
$3d^5 4s4p\ ^5P_2$	$3d^5 4s\ ^7S_3$	71.3	72.9	0.101	0.111		$3d^5 4s\ ^5G_6$			0.42	0.29
	$3d^5 4s\ ^5S_2$			3.80	2.75		$3d^5 4s\ ^5G_5$			0.044	0.025
	$3d^4 4s^2\ ^5D_1$			0.85	1.16						
	$3d^4 4s^2\ ^5D_2$			3.39	4.02						
	$3d^4 4s^2\ ^5D_3$			5.04	5.68						

Table 3 lists the calculated energies for the lowest 50 *LS* states of Cr II and compares the predicted results with the experimental values [24] (the full list of the 194 *LS* states involved into photoionization calculations is given in Supplementary Materials). Again, the residual Cr II ionic target states were determined by using term-dependent non-orthogonal orbitals in the MCHF approach and by accounting for all important correlation effects through properly chosen important configurations. The convergence of the target expansions for Cr II is noted to be faster than for the neutral chromium. The cut-off parameters were chosen to take balanced account of correlation effects in the initial bound states of neutral chromium and the residual singly-ionized chromium states, and thus to obtain the best possible agreement with the experimental photoionization thresholds. The balance in correlation effects between the initial and final states is important for the correct positions and shapes of resonance structures. As seen from Table 3, the agreement between the predicted and observed *LS* energies is better than 0.1 eV for most states, except for some doublet terms where the convergence was found to be very slow. Note that the same Cr II wave functions, with addition of spin-orbit mixing, were used in our recent calculations of electron scattering from Cr II [23]. The discussions of the quality of the target wave functions presented in Cr II paper is also applied to the present model. In particular, the agreement of transition probabilities for E1 transitions with experiment was found to be very satisfactory, with an overall dispersion of 8.3% with the experimental results of Nilsson et al. [28] and 10.1% with Lawler et al. [29]. The good agreement with experiments supports the accuracy of our target wave function expansions.

Table 3. Excitation energies (in eV) of the final residual Cr II states included into close-coupling expansions.

Index	Config.	Term	Present	NIST	Diff.
1	$3d^5$	$a\,^6S$	0.00000	0.00000	0.000
2	$3d^4(^5D)4s$	$a\,^6D$	1.52326	1.52226	0.001
3	$3d^4(^5D)4s$	$a\,^4D$	2.45936	2.45836	0.001
4	$3d^5$	$a\,^4G$	2.54358	2.54358	−0.000
5	$3d^5$	$a\,^4P$	2.70874	2.70574	0.003
6	$3d^5$	$b\,^4D$	3.10351	3.10451	−0.001
7	$3d^5$	$a\,^2I$	3.73773	3.73773	0.000
8	$3d^4(^3P)4s$	$b\,^4P$	3.78582	3.78482	0.001
9	$3d^4(^3H)4s$	$a\,^4H$	3.81119	3.75477	0.056
10	$3d^4(^3F)4s$	$a\,^4F$	3.86778	3.86378	0.004
11	$3d^5$	$a\,^2D$	3.90995	3.89595	0.014
12	$3d^5$	$b\,^4F$	4.07063	4.07263	−0.002
13	$3d^4(^3G)4s$	$b\,^4G$	4.16148	4.16448	−0.003
14	$3d^5$	$a\,^2F$	4.18702	4.02475	0.162
15	$3d^4(^3H)4s$	$a\,^2H$	4.30700	4.30600	0.001
16	$3d^4(^3P)4s$	$a\,^2P$	4.35478	4.35478	0.000
17	$3d^4(^3F)4s$	$b\,^2F$	4.41673	4.41273	0.004
18	$3d^5$	$b\,^2H$	4.42169	4.42169	0.000
19	$3d^5$	$a\,^2G$	4.47980	4.48780	−0.008
20	$3d^4(^3D)4s$	$c\,^4D$	4.75038	4.75038	−0.000
21	$3d^4(^3G)4s$	$b\,^2G$	4.77322	4.77822	−0.005
22	$3d^4(^1I)4s$	$b\,^2I$	4.98292	4.98592	−0.003
23	$3d^4(^1S)4s$	$a\,^2S$	5.00483	5.01083	−0.006
24	$3d^4(^1G)4s$	$c\,^2G$	5.07723	4.92984	0.147
25	$3d^5$	$c\,^2F$	5.08334	4.93695	0.146
26	$3d^4(^3D)4s$	$b\,^2D$	5.50234	5.32306	0.179
27	$3d^5$	$b\,^2S$	5.60739	5.49338	0.114
28	$3d^4(^1D)4s$	$c\,^2D$	5.74380	5.66684	0.077
29	$3d^4(^5D)4p$	$z\,^6F^o$	5.87151	5.87151	−0.000
30	$3d^4(^5D)4p$	$z\,^6P^o$	5.93772	6.01735	−0.080
31	$3d^4(^5D)4p$	$z\,^6D^o$	5.96387	6.15335	−0.189
32	$3d^4(^5D)4p$	$z\,^4P^o$	6.11507	6.11407	0.001
33	$3d^5$	$d\,^2D$	6.12220	5.87209	0.250
34	$3d^4(^5D)4p$	$z\,^4F^o$	6.42101	6.42101	0.000
35	$3d^4(^1F)4s$	$d\,^2F$	6.44629	6.28302	0.163
36	$3d^5$	$d\,^2G$	6.61223	6.48570	0.127
37	$3d^34s^2$	$c\,^4F$	6.64022	6.64022	−0.000
38	$3d^4(^5D)4p$	$z\,^4D^o$	6.77489	6.77489	−0.000
39	$3d^4(^3P)4s$	$c\,^4P$	6.84797	6.84997	−0.002
40	$3d^4(^3F)4s$	$d\,^4F$	6.85529	6.80387	0.051
41	$3d^4(^3P)4s$	$b\,^2P$	7.34461	7.34761	−0.003
42	$3d^4(^3F)4s$	$e\,^2F$	7.38416	7.38616	−0.002
43	$3d^4(^3H)4p$	$z\,^4H^o$	7.67458	7.91380	−0.239
44	$3d^4(^3P)4p$	$y\,^4D^o$	7.99860	7.99660	0.002
45	$3d^4(^1G)4s$	$e\,^2G$	8.02488	7.77314	0.252
46	$3d^4(^3P)4p$	$z\,^2S^o$	8.08561	8.06261	0.023
47	$3d^4(^3H)4p$	$z\,^4I^o$	8.10058	8.12779	−0.027
48	$3d^4(^3F)4p$	$z\,^4G^o$	8.11882	8.11182	0.007
49	$3d^4(^3P)4p$	$y\,^4P^o$	8.12608	8.24797	−0.122
50	$3d^4(^3H)4p$	$z\,^2G^o$	8.13573	8.13573	0.000
...					
194	$3d^3(^2D)4s4p$	$^2P^o$	20.72358		

2.2. Photoionization Calculations

The parallelized version of the BSR code [16] based on the *R*-matrix method to solve the close-coupling equations has been employed in the photoionization calculation. The *B*-splines are used as a universal basis to represent the continuum wave functions in the inner region, $r \leq a$. The *R*-matrix expansion in the inner region takes the form

$$\Psi_k(x_1,\ldots,x_{N+1}) = \mathcal{A}\sum_{ij}\bar{\Phi}_i(x_1,\ldots,x_N;\hat{\mathbf{r}}_{N+1}\sigma_{N+1})\,r_{N+1}^{-1}\,B_j(r_{N+1})\,a_{ijk} + \sum_i \chi_i(x_1,\ldots,x_{N+1})\,b_{ik}\,. \quad (1)$$

Here $\mathcal{A}$ denotes the antisymmetrization operator, $\bar{\Phi}_i$ are the channel functions, and the splines $B_j(r)$ represent the continuum wave functions. The B-splines form an effectively complete basis with no requirement of Buttle correction to the R-matrix. The amplitudes of the wave functions at the boundary are given by the coefficient of the last spline. We impose only limited orthogonality conditions between the bound and continuum orbitals. In the present calculations, the orthogonality of the continuum orbitals to the bound orbitals in the closed $1s$, $2s$, $2p$, $3s$, and $3p$ subshells was imposed and no orthogonality constraints were imposed to the other spectroscopic orbitals or the correlated orbitals. As a consequence, the $(N+1)$-electron configurations χ_i in the second part of Equation (1) can be completely avoided. This allowed us to keep a balance between the scattering and bound parts of the close-coupling expansions and, therefore, to avoid the pseudo-resonance structure. The inconsistency between the scattering and bound parts of the close-coupling expansions can give rise to the pseudo-resonance structures.

The close-coupling expansion Equation (1) includes the 194 states of singly ionized chromium. Some of these states lie above the ionization threshold, particularly the states belonging to the $3d^3 4s4p$ configuration. These states may have a large influence on the resonant photoionization process due to the strong $3d-4p$ and $4s-4p$ dipole transitions. The present photoionization model is referred to as BSR-194 in the discussion below. The BSR-194 model contained up to 591 different scattering channels in the LS-coupling scheme. The inner region boundary radius was chosen to be $20\,a_0$ (where $a_0 = 0.529 \times 10^{-10}$ m is the Bohr radius). The continuum wave functions were represented by 86 B-splines of order 8. The complicated aspects of the present photoionization calculations are the large configuration expansions for the total scattering functions (∼100,000 terms) and the extremely large number of two-electron matrix elements to be calculated. This is partly caused by the open $3d$ subshell configurations of the atomic systems, however, the major complication originates in the huge number of overlap factors due to the use of nonorthogonal orbital sets. Further optimization of the code for the determination of the angular coefficients and the subsequent construction of the Hamiltonian matrix was carried out to handle these computational issues of the present calculations. More detailed descriptions of the present computational procedure can be found in our recent calculations for photoionization of Fe I [17].

The R-matrix theory of photoionization is described by the dipole matrix elements between the initial state Ψ_0 and the R-matrix basis states Ψ_k. The radial wave functions of the initial bound states are well confined to the inner region. The total photoionization cross section for an initial bound state of total orbital angular momentum L_0 is defined as a function of photon energy ω (in Rydberg) as follows

$$\sigma(\omega) = \frac{8}{3}\pi^2\,\alpha\,\omega^{\pm 1}\,\frac{1}{(2L_0+1)}\sum_j |(\Psi_j^-\|D\|\Psi_0)|^2, \tag{2}$$

where D is the electric dipole operator and α is the fine-structure constant. The length and velocity forms of photoionization cross sections are given by the powers of ω = +1 and $\omega = -1$, respectively. The summation is taken over the various open channels j. The wave functions Ψ_j^- are subjected to asymptotic conditions with a plane wave in the direction of the ejected electron momentum k and ingoing waves in all open channels. The functions Ψ_j^- are expressed in terms of the R-matrix states, and the program ASYPCK [30] is used to generate the asymptotic solutions and to find the expansion coefficients for the Ψ_j^-.

3. Results and Discussion

The total photoionization cross sections for the ground $3d^5 4s\ ^7S$ state of neutral chromium is displayed in panel (a) of Figure 1 as a function of photon energy from the Cr II $3d^5\ a^6S$ ionization threshold to 30 eV. Both the length and velocity forms are shown. As seen from the Figure, there is a close agreement (within 10%) between the two forms. This indicates the good convergence of the configuration expansions used for the initial bound and final ionic states. The same level of agreement between length and velocity forms is also observed for all photoionization cross sections from the

excited states of Cr I discussed below. The photoionization cross sections exhibit rich resonance structures. In order to delineate the autoionization resonances near the ionization thresholds, we used a fine energy step of 1.36×10^{-3} eV up to the highest ionization threshold around 26 eV. This covers all states of the residual Cr II ion considered in the present work. The resonance structure is made up of a few wide and strong resonances at lower photon energies and many narrow and intense resonances over a wide range of photon energies. The distinctive feature of the photoionization cross sections is the almost zero background until the first excited ionic $3d^4(^5D)4s\ ^6D$ threshold is reached at 8.29 eV above the ionization threshold.

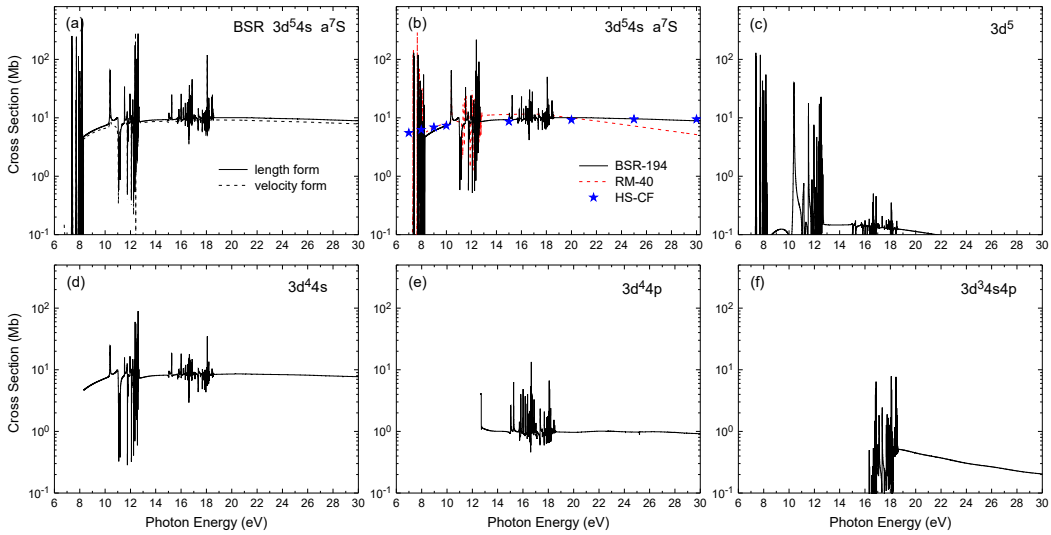

Figure 1. Total and partial photoionization cross sections from the ground $3d^4 4s\ ^7S$ state of Cr I as a function of photon energy. Panel (**a**) shows total cross sections from the present BSR-194 model in the length and velocity forms. Panel (**b**) compares the BSR-194 model with the RM-40 calculation of Nahar [14] and with Hartree-Slater central-field (HF-CF) calculation of Reilman and Manson [12]. Panels (**c**–**f**) show summed partial cross sections for leaving the residual Cr II ion in final states of the $3d^5$, $3d^4 4s$, $3d^4 4p$, and $3d^3 4s 4p$ configurations.

The total photoionization cross sections from the most recent 40-states *R*-matrix calculations of Nahar [14] are compared with the present results in panel (**b**). This model is referred to as RM-40 in the discussion below. There is close agreement between the present BSR-194 calculations and the RM-40 results for the background cross sections at lower energies. However, there are discrepancies in resonance structures, especially at higher energies, where BSR-194 and RM-40 models noticeable differences in the position, width, and magnitude of resonances. Additional resonance features converging on higher Cr II thresholds included in present calculations can be clearly seen. The deviations between the two calculations are due to the differences in wave functions to represent Cr I initial bound, final continuum states, and Cr II residual ionic thresholds. The differences in the positions of the resonances are related to the different positions of the ionization thresholds. As discussed above, the present ionization thresholds generally agree with the experimental values to better than 0.1 eV. The photoionization at higher energies requires access to higher Cr II excited states that lie above the first ionization threshold at 16.49 eV. Most of these highly excited states belong to the $3d^3 4s 4p$ configuration and some to the $3d^4 4p$ configuration. The resonances in this energy region are weaker than the resonances in the low energy region.

The panel (**b**) also provide the comparison with early calculations by Reilman and Manson (1979) carried out in the Hartree-Slater central-field approximation on each individual sub-shell. This approach does not reproduce any resonance structure, however, can accurately produce the background cross sections which closely agree with the present calculation. The RM-40 cross

sections decrease more rapidly above 20 eV due to the absence of high-lying $3d^3 4s4p$ states in the close-coupling expansion.

The nonlocal thermodynamic equilibrium modeling calculations of astrophysical plasmas need accurate determination of the population of the excited levels of the residual ion following the photoionization process. The partial photoionization cross sections for leaving the residual ion in various states from both the ground and the low-lying excited states are then required. Our calculations show that the photoionization of Cr I populate many residual final ionic states. Generally there is no dominant ionic channel in the photoionization of a given initial state because of the complex Cr II structure. The configurations with an open $3d$ subshell results in many final ionic states with different total and intermediate terms. The partial photoionization cross sections from the ground $3d^5 4s\ ^7S$ state for leaving the residual Cr II ion in final states of the $3d^5$, $3d^4 4s$, $3d^4 4p$, and $3d^3 4s4p$ configurations have been presented in panels (c–f) of Figure 1. The summed partial cross sections from various states of Cr II belonging to a given configuration have been presented in the Figure due to a large number of final ionic states. However, the partial photoionization cross sections for all individual states of Cr II belonging to these configurations are available in electronic tables upon request.

The dominant channels in the photoionization of the ground state $3d^5 4s\ ^7S$ at near-threshold energies are due to photoionization of the $4s$ electron which leads to final ionic states with the $3d^5$ configuration. The detailed comparison of the partial cross sections leaving the residual ion in various terms of the $3d^5$ configuration shows that the ionization to the $3d^5\ ^6S$ Cr II ground state dominates in the summed partial cross sections. These channels also exhibit strong resonance structures. The $3d$ ionization channels open up above 8.29 eV and ionization to final ionic states with configuration $3d^4 4s$ becomes dominant, leading to the big step-like enhancement in the total photoionization cross sections. These channels mostly determine the magnitude of the total photoionization cross sections at higher energies. As shown in the other panels, ionization with additional excitation to the $3d^4 4p$ and $3d^3 4s4p$ final ionic states is also noticeable. This process is expected to be important due to the strong $4s - 4p$ and $3d - 4p$ transitions in the ionic states. These cross sections exhibit a different energy dependence of the background and their overall contribution to the total photoionization is about 10% or less. Note that the partial cross sections to the $3d^3 4s^2$ final ionic states were found to be very small and, therefore, are not shown in the Figure. Such transitions are not possible in one-electron approximation and may occur only due to channel coupling or the decay of resonances into these states.

The total and partial photoionization cross sections for the Cr I first excited state $3d^5 4s\ ^5S$ are shown in Figure 2. This state has the same configuration as the ground state, however, due to less restriction imposed by spin consideration the number of final ionic states increases and it leads to more intense resonance structure over a wide energy range. Ionization of the $4s$ electron again leads to the $3d^5$ final ionic states, with a set of prominent resonances, but with considerable background continuum cross sections in this case. The $3d$ electron ionization with the $3d^4 4s$ final ionic states again dominates for all energies. Photoionization with excitation becomes more important here and leads to noticeable population of the $3d^4 4p$ and $3d^3 4s4p$ final ionic states. The panels (c–f) of Figure 2 show the summed partial photoionization cross sections in numerous individual final ionic states but generally have no dominant ionization channel. The overall agreement with the RM-40 calculations [14] is generally very good, except the present cross sections show stronger resonance structure and bigger magnitude of the background cross sections at higher energies. This is due to a larger number of final ionic states included in the present close-coupling expansions, in particular, the additional ionic states of the $3d^4 4p$ and $3d^3 4s4p$ configurations.

The photoionization cross sections of even-parity $3d^4 4s^2\ ^5D$ excited state are displayed in Figure 3. The populations of the final ionic states change considerably in comparison to the previous examples for states with the $3d^5 4s$ configuration. At lower energies, $4s$ electron ionization provides the dominant channels, leading to final ionic states with configuration $3d^4 4s$. These channels also exhibit the strong resonance structure. The $3d$ ionization channels open up above 12 eV, and ionization to final ionic states with configuration $3d^3 4s^2$ becomes dominant. These channels

define the magnitude of the total photoionization cross sections at higher energies. As illustrated in other panels, ionization with additional excitation to the $3d^4 4p$ and $3d^3 4s4p$ final ionic states is also noticeable, providing considerable contributions to both the resonance structure and background continuum. The background cross sections exhibit a different energy dependence in this case. Ionization of the $4s$ electron with excitation to the $3d^4 4p$ final ionic states shows a near-threshold maximum with subsequent decrease in value, whereas $3d$ ionization with excitation to the $3d^3 4s4p$ final ionic states shows increasing cross sections over a wide range of energies. The qualitative agreement with the RM-40 calculations of Nahar (2009) was found only for the low near-threshold energies. At higher energies, the RM-40 cross sections quickly decrease whereas the present BSR-194 cross sections show approximately constant background cross sections. From the partial contributions presented in the Figure 3, we may conclude that the RM-40 close-coupling expansions missed some important final ionic states, especially the higher-lying states with the $3d^3 4s^2$ and $3d^4 4p$ configurations.

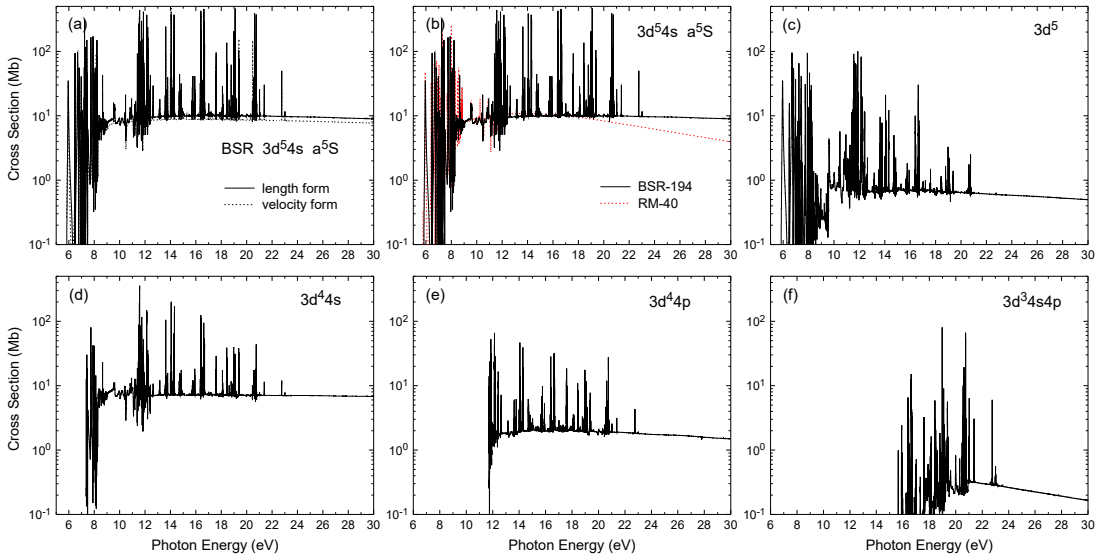

Figure 2. Total and partial photoionization cross sections from the excited $3d^4 4s\ ^5S$ state of Cr I as a function of photon energy. Panel (**a**) shows total cross sections from the present BSR-194 model in the length and velocity forms. Panel (**b**) compares the BSR-194 model with the RM-40 calculation of Nahar [14]. Panels (**c**–**f**) show summed partial cross sections for leaving the residual Cr II ion in final states of the $3d^5$, $3d^4 4s$, $3d^4 4p$, and $3d^3 4s4p$ configurations, respectively.

We now turn to discuss the photoionization of the odd-parity $3d^5 4p$ and $3d^4 4s4p$ states of Cr I. As example, Figure 4 presents total and partial cross sections for the $3d^5 4p\ z^5P$ bound state. In this case, $4p$ electron ionization leads to the $3d^5$ ionic states and contributes mainly in the near-threshold region. The main contribution at higher energies is again due to the $3d$ electron ionization leading to the $3d^4 4p$ ionic states. We also see considerable contribution of the $3d^4 4s$ channels, which is due to the close-coupling effects and strong configuration mixing of the ionic states. The $3d^3 4s4p$ ionic states are populated mainly through resonant excitation. The present cross sections show stronger resonance structures than the RM-40 model. The background cross sections at higher energies exhibit differences in both shape and magnitude.

Photoionization from the excited $3d^4 4s4p\ y\ ^5P$ bound state is illustrated in Figure 5. The $3d^4 4s4p$ states have three main photoionization channels related to the ionization of the $3d$, $4s$, or $4p$ electrons. Ionization of the outer $4p$ electron leads mostly to the $3d^4 4s$ final ionic states. As seen from the Figure, the corresponding partial cross sections provide the main contribution in the near-threshold region, but the magnitude quickly decreases with increasing energy. The ionization of the $4s$ electron leads in this case to the $3d^4 4p$ ionic states. The background cross sections for these ionic states change slowly

with energy. On an average, the contribution from the 4*s* electron ionization to the total cross section is ∼20%. The main contribution to the total cross sections at higher energies originates from the 3*d* electron ionization, which leads to the $3d^3 4s4p$ final ionic states. Omission of these states in the RM-40 calculation is likely the main reason for the differences at higher energies. The contribution of the $3d^5$ channels is also significant and results mainly in additional resonance structure. The background cross section here is due to close-coupling effects and quickly decreases with energy.

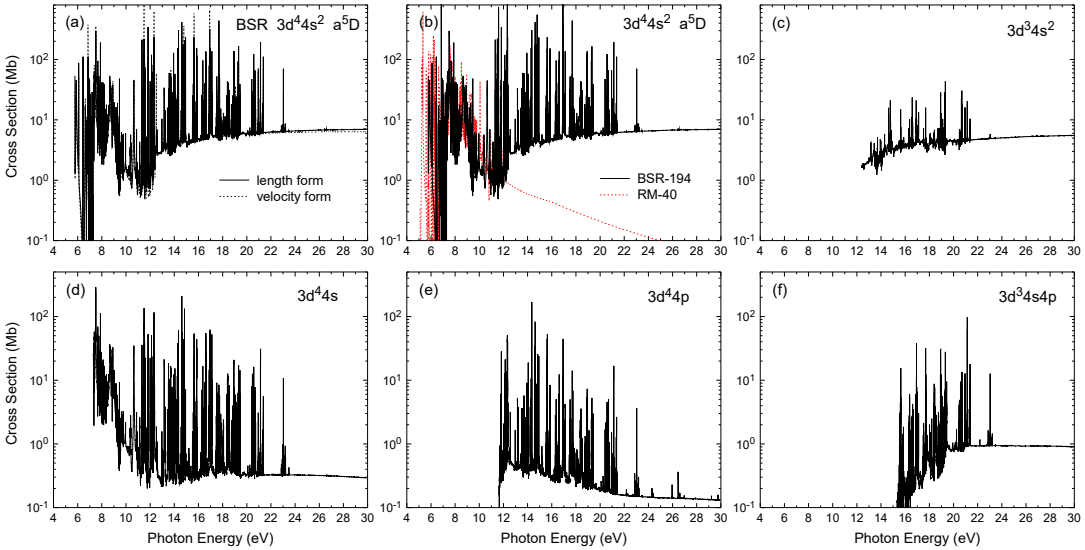

Figure 3. Total and partial photoionization cross sections from the excited $3d^4 4s^2\ ^5D$ state of Cr I as a function of photon energy. Panel (**a**) shows total cross sections from the present BSR-194 model in the length and velocity forms. Panel (**b**) compares the BSR-194 model with the RM-40 calculation of Nahar [14]. Panels (**c**–**f**) show summed partial cross sections for leaving the residual Cr II ion in final states of the $3d^5$, $3d^4 4s$, $3d^4 4p$, and $3d^3 4s4p$ configurations, respectively.

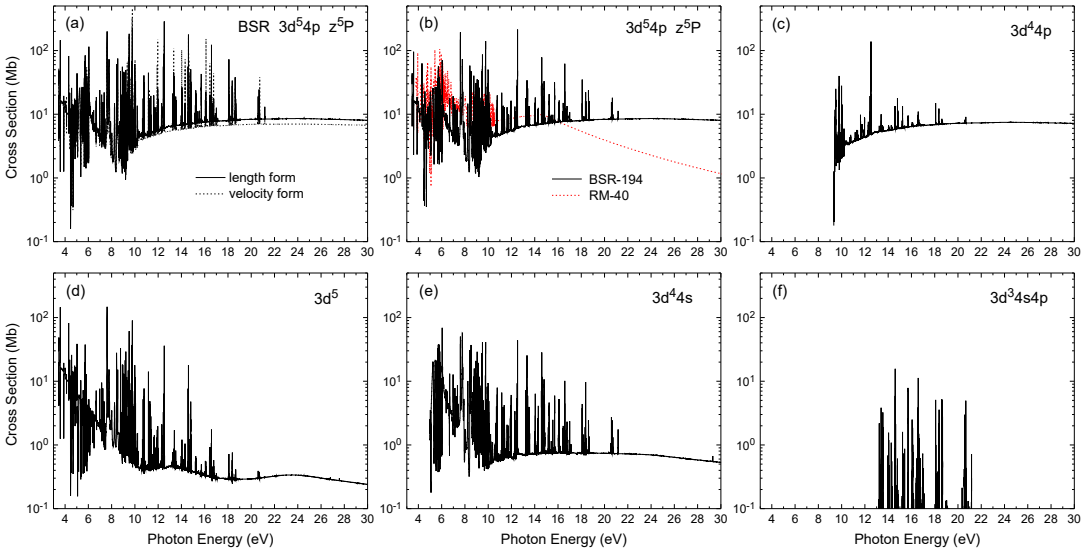

Figure 4. Total and partial photoionization cross sections from the excited $3d^5 4p\ z^5P$ state of Cr I as a function of photon energy. Panel (**a**) shows total cross sections from the present BSR-194 model in the length and velocity forms. Panel (**b**) compares the BSR-194 model with the RM-40 calculations of Nahar [14]. Panels (**c**–**f**) show summed partial cross sections for leaving the residual Cr II ion in final states of the $3d^5$, $3d^4 4s$, $3d^4 4p$, and $3d^3 4s4p$ configurations, respectively.

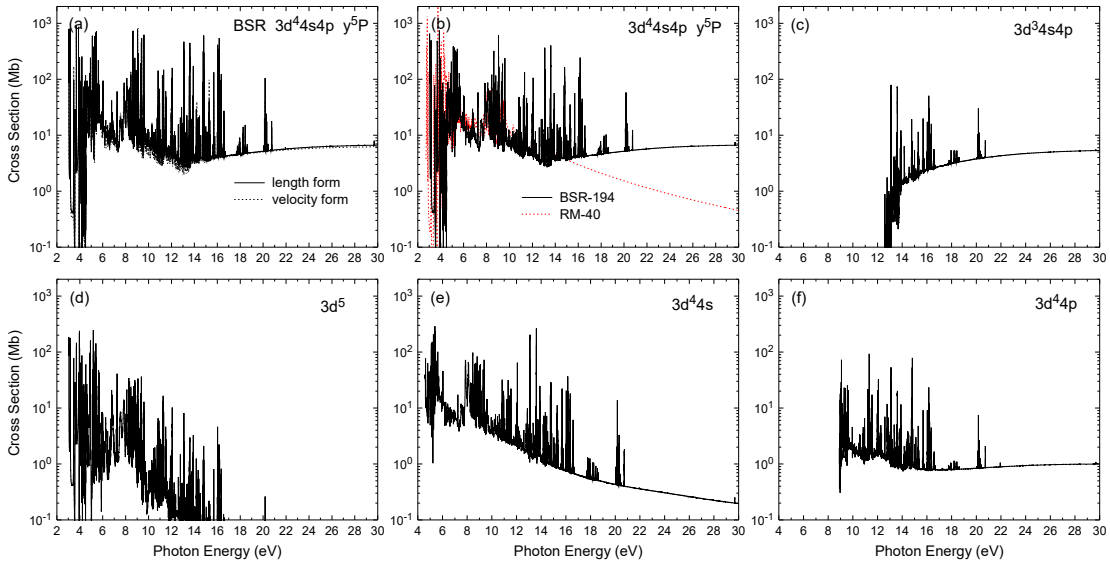

Figure 5. Total and partial photoionization cross sections from the excited $3d^5 4p\ y^5P$ state of Cr I as a function of photon energy. Panel (**a**) shows total cross sections from the present BSR-194 model in the length and velocity forms. Panel (**b**) compares the BSR-194 model with the RM-40 calculations of Nahar [14]. Panels (**c**–**f**) show summed partial cross sections for leaving the residual Cr II ion in final states of the $3d^5$, $3d^4 4s$, $3d^4 4p$, and $3d^3 4s4p$ configurations, respectively.

It is clear from the above discussion that the photoionization of neutral chromium leads to numerous residual ionic states. The relative population of the ionic states changes considerably with the photon energy. The background cross sections for photoionization from the ground and excited states are very similar both in shape and magnitude. As discussed above, the background cross sections are mainly defined by direct ionization of the $3d$ electron and, therefore, all of them have approximately the same value of about 10 Mb at higher energies.

4. Conclusions

The total and partial photoionization cross sections of Cr I leading to various final Cr II ionic states due to the ejection of $3d$, $4s$, and $4p$ photoelectrons and photoionization with excitation have been investigated in the low-energy region up to 30 eV. We present the photoionization cross sections for the 20 bound states of Cr I with configurations $3d^5 4s$, $3d^4 4s^2$, $3d^5 4p$, and $3d^4 4s4p$. These examples cover all principal configurations and angular symmetries of neutral chromium.

The calculations were performed with the modified version of the *B*-spline *R*-matrix code [16] to solve the close-coupling equations. For the representation of the initial bound and final ionic states, we used extensive multiconfiguration expansions with carefully chosen configurations. The correlation effects have been accurately accounted for by employing term-dependent non-orthogonal one-electron radial wave functions. Thus we were able to generate a more accurate description of the initial bound and final ionic states than those employed in previous works. Our calculated lifetimes and transition probabilities between fine-structure of the Cr I bound states show good agreement with highly accurate measured values. Excellent agreement between the present photoionization cross sections in length and velocity formulations also attests to the high quality of wave functions.

The present calculations aimed to check the convergence of the photoionization cross sections and adopted a much larger set of final ionic states in the close-coupling expansion than in previous works. The photoionization of valence $3d$, $4s$, and $4p$ electrons from the atomic chromium leads to the final singly-ionized chromium terms of the $3d^4 4s$, $3d^3 4s^2$, $3d^5$, $3d^4 4p$, and $3d^3 4s4p$ configurations. We have included all 194 *LS* states of these ionic configurations and, therefore, our close-coupling expansions cover all major photoionization channels. The predicted photoionization cross sections are

in reasonable agreement with the available *R*-matrix calculations [14], however, for higher-lying states there are significant differences, both in the resonance structure and the background cross sections.

The photoionization of excited bound states of Cr I exhibits numerous scattering channels. We performed a detailed analysis of the different photoionization channels, showing that the relative population of the different ionic states changes considerably with the variation in photon energy. In particular, we found that 3*d* ionization becomes the dominant channel at higher photon energies. This leads to approximately the same value of the background photoionization cross sections for all Cr I bound states. In addition, we carefully delineated the autoionizing resonance structures. The atomic data reported here are important for the interpretation and modeling of spectra from the stellar and nebular objects. The numerical data for the total and partial cross sections are available in electronic form upon request.

Supplementary Materials: The following are available online at http://www.mdpi.com/2218-2004/8/3/51/s1, Table S1: Excitation energies of the final residual Cr II states.

Author Contributions: Both authors contributed to the writing of the text. All authors have read and agreed to the published version of the manuscript.

Funding: This work was supported by the United States National Science Foundation under grants No. AST-1714159 (ST) and No. PHY-1834740 (OZ). The numerical calculations were performed on STAMPEDE II at the Texas Advanced Computing Center. They were made possible through the XSEDE allocations No. PHY-170047 (ST) and No. PHY-090031 (OZ).

Conflicts of Interest: The authors declare no conflict of interest.

Abbreviations

The following abbreviations are used in this manuscript:

MDPI	Multidisciplinary Digital Publishing Institute
MCHF	Multi-configuration Hartree-Fock
RM	*R*-matrix
BSR	*B*-spline *R*-matrix

References

1. Barklem, C.; Chrislib, N.; Beers, T.C.; Hill, V.; Bessell, M.S.; Holmberg, J.; Marsteller, B.; Rossi, S.; Zickgraf, F.-J.; Reimers, D. The Hamburg/ESO R-process enhanced star survey (HERES)-II. Spectroscopic analysis of the survey sample. *Astron. Astrophys.* **2005**, *439*, 129–151. [CrossRef] [CrossRef]
2. Dimitrijevíc, M.S.; Ryabchikova, T.; Simíc, Z.; Popovíc, L.C.; Dacíc, M. The influence of Stark broadening on Crspectral line shapes in stellar atmospheres. *Astron. Astrophys.* **2007**, *469*, 681–686. [CrossRef] [CrossRef]
3. Wallace, L.; Hinkle, K. The 236.6–5400.0 nm spectrum of Cr I. *Astrophys. J.* **2009**, *700*, 720–726. [CrossRef] [CrossRef]
4. Martins, M.; Godehusen, K.; Richter, T.; Wernet, P.; Zimmermann, P. Open shells and multi-electron interactions: Core level photoionization of the 3d metal atoms. *J. Phys. B At. Mol. Opt. Phys.* **2006**, *39*, R79–R125. [CrossRef] [CrossRef]
5. Bruhn, R.; Schmidt, E.; Schröder, H.; Sonntag, B. VUV photoabsorption and photoemission of atomic Cr. *J. Phys. B At. Mol. Opt. Phys.* **1982**, *15*, 2807–2817. [CrossRef] [CrossRef]
6. Cooper, J.W.; Clark, C.W.; Cromer, C.R.; Lucatorto, T.B.; Sonntag, B.F.; Kennedy, E.T.; Costello, J.T. Marked differences in the 3p photoabsorption between the Cr and Mn^+ isoelectronic pair: Reasons for the unique structure observed in Cr. *Phys. Rev. A* **1989**, *39*, 6074–6077. [CrossRef] [CrossRef]
7. Costello, J.T.; Kennedy, E.T.; Sonntag, B.F.; Clark, C.W. 3p photoabsorption of free and bound Cr, Cr^+, Mn, and Mn^+. *Phys. Rev. A* **1991**, *43*, 1441–1450. [CrossRef] [CrossRef]
8. Godehusen, K.; Richter, T.; Zimmermann, P.; Martins, M. Ion-charge resolved 3p photoabsorption measurements of atomic Cr. *J. Phys. B At. Mol. Opt. Phys.* **2003**, *36*, L387–L392. [CrossRef] [CrossRef]
9. Osawa, T.; Kawajiri, K.; Suzuki, N.; Nagata, T.; Azuma, Y.; Koike, F. Photoion-yield study of the 3p–3d giant resonance excitation region of isolated Cr, Mn and Fe atoms. *J. Phys. B At. Mol. Opt. Phys.* **2012**, *45*, 225204. [CrossRef] [CrossRef]

10. Dolmatov, V.K. The case of a unique autoionization decay dynamic: The 3p to nd resonances in Cr. *J. Phys. B At. Mol. Opt. Phys.* **1993**, *26*, L393–L398. [CrossRef] [CrossRef]
11. Donnelly, D.; Bell, K.L.; Hibbert, A. The 3p-photoabsorption of chromium. *J. Phys. B At. Mol. Opt. Phys.* **1996**, *29*, L693–L697. [CrossRef] [CrossRef]
12. Reilman, R.F.; Manson, S.T. Photoabsorption Cross Sections for Positive Ions with Z <= 30. *Astrophys. J. Suppl. Ser.* **1979**, *40*, 815–880. [CrossRef]
13. Verner, D.; Yakovlev, D.; Band, I.; Trzhaskovskaya, M. Subshell photoabsorption cross cections and ionization energies of atoms and ions from He to Zn. *ADNDT* **1993**, *55*, 233–280, doi:10.1088/0953-4075/26/14/003. [CrossRef]
14. Nahar, S.N. Photoionization and electron–ion recombination of Cr I. *J. Quant. Spectrosc. Radiat. Transf.* **2009**, *110*, 2148–2161. [CrossRef] [CrossRef]
15. Berrington, K.A.; Eissner, W.B.; Norrington, P.H. RMATRX1: Belfast atomic *R*-matrix codes. *Comput. Phys. Commun.* **1995**, *92*, 290–420. [CrossRef] [CrossRef]
16. Zatsarinny, O. BSR: *B*-spline atomic *R*-matrix codes. *Comput. Phys. Commun.* **2006**, *174*, 273–356. [CrossRef] [CrossRef]
17. Zatsarinny, O.; Bartschat, K.; Fernandez-Menchero, L.; Tayal, S.S. Photoionization of neutral iron from the ground and excited states. *Phys. Rev. A* **2019**, *99*, 023430. [CrossRef] [CrossRef]
18. Tayal, S.S.; Zatsarinny, O. Electron-impact excitation of forbidden and allowed transitions in Fe II. *Phys. Rev. A* **2018**, *98*, 012706. [CrossRef] [CrossRef]
19. Wang, K.; Zatsarinny, O.; Bartschat, K. Electron Scattering from Neutral Fe and Low-energy Photodetachment of Fe^-. *Astrophys. J.* **2018**, *867*, 63. [CrossRef] [CrossRef]
20. Froese Fischer, C.; Tachiev, G.; Gaigalas, G.; Godefroid, M.R. An MCHF atomic-structure package for large-scale calculations. *Comput. Phys. Commun.* **2007**, *176*, 559–579. [CrossRef] [CrossRef]
21. Zatsarinny, O.; Froese Fischer, C. A general program for computing angular integrals of the Breit–Pauli Hamiltonian with non-orthogonal orbitals. *Comput. Phys. Commun.* **2000**, *12*, 247–289. [CrossRef] [CrossRef]
22. Zatsarinny, O.; Froese Fischer, C. Atomic structure calculations using MCHF and BSR. *Comput. Phys. Commun.* **2009**, *180*, 2041–2065. [CrossRef] [CrossRef]
23. Tayal, S.S.; Zatsarinny, O. Collision and Radiative Parameters for Cr ii Lines Observed in Stellar and Nebular Spectra. *Astrophys. J.* **2020**, *888*, 10. [CrossRef] [CrossRef]
24. Kramida, A.; Ralchenko, Y.; Reader, J.; NIST ASD Team. *NIST Atomic Spectra Database (Version 5.3)*; National Institute of Standards and Technology: Gaithersburg, MD, USA, 2015. Available online: http://physics.nist.gov/asd (accessed on 28 April 2016).
25. Scott, P.; Asplund, M.; Grevesse, N.; Bergemann, M.; Jacques, S.A. The elemental composition of the Sun-II. The iron group elements Sc to Ni. *Astron. Astrophys.* **2015**, *573*, A26. [CrossRef] [CrossRef]
26. Sobeck, J.S.; Lawler, J.E.; Sneden, C. Improved Laboratory Transition Probabilities for Neutral Chromium and Redetermination of the Chromium Abundance for the Sun and Three Stars. *Astrophys. J.* **2007**, *667*, 1267–1282. [CrossRef] [CrossRef]
27. Cooper, J.C.; Gibson, N.D.; Lawler, J.E. Radiative lifetimes in Cr I by laser induced fluorescence. *J. Quant. Spectrosc. Radiat. Transf.* **1997**, *58*, 85–92. [CrossRef] [CrossRef]
28. Nilsson, H.; Ljung, G.; Lundberg, H.; Nielsen, K.E. The FERRUM project: Improved experimental oscillator strengths in Cr. *Astron. Astrophys.* **2006**, *445*, 1165–1168. [CrossRef] [CrossRef]
29. Lawler, J.E.; Sneden, C.; Nave, G.; Den Hartog, E.A.; Emrahoğlu, N.; Cowan, J.J. Improved Cr II log(gf) values and abundance determinations in the photosheres of the sun and meta–poor star HD 84937. *Astrophys. J. Suppl. Ser.* **2017**, *228*, 10. [CrossRef] [CrossRef]
30. Crees, M.A. ASYPCK, a program for calculating asymptotic solutions of the coupled equations of electron collision theory. *Comput. Phys. Commun.* **1980**, *19*, 103–137. [CrossRef] [CrossRef]